Magnetoreflection and magnetophotoluminescence in the dilute magnetic semiconductor $Zn_{1-x}Mn_xTe$

Le Van Khoi,* R. R. Gałązka, and W. Zawadzki
Institute of Physics, Polish Academy of Sciences, Al. Lotnikow 32/46, 02-668 Warsaw, Poland

(Received 2 February 2018; revised manuscript received 20 April 2018; published 28 June 2018)

Magnetoreflection (MR) and magnetophotoluminescence (MPL) are studied in the diluted magnetic semiconductor $Zn_{1-x}Mn_xTe$. The use of both methods in parallel allows us to follow features resulting from the mean-field exchange behavior as well as individual characteristics of Mn^{2+} paramagnetic ions. Resonance linewidths observed in MR are analyzed and shown to depend on spin-dependent scattering of excitons. A striking feature of the MPL spectrum is an enhancement of *all* spin-polarized luminescence structures in an external magnetic field. Relations between the Zeeman energy shift of exciton transitions due to exchange interaction of Mn ions with mobile carriers and circular polarization of MPL due to internal recombination in Mn^{2+} are revealed. Mixing of left and right circular light polarizations is demonstrated in excitonic and donor-acceptor pair (DAP) structures of MPL peaks. An enhancement of binding energy with increasing magnetic field for excitons localized by potential fluctuations is demonstrated and explained. It is observed that the energy of MPL peaks related to DAPs is only weakly sensitive to magnetic field. This relative stability is caused by a suppression of the mean-field Zeeman shift due to the two-component form of impurity wave functions. The simultaneous presence of paramagnetic ions and residual nonmagnetic impurities in our $Zn_{1-x}Mn_xTe$ samples provides for a rich physical picture.

DOI: 10.1103/PhysRevB.97.214435

I. INTRODUCTION

Dilute magnetic semiconductors (DMSs), also called semimagnetic semiconductors, have been a subject of sustained experimental and theoretical investigations since their discovery 40 years ago. This well-defined family of materials is formed by adding substitutionally paramagnetic ions (mostly Mn^{2+}) to nonmagnetic semiconducting compounds. With their distinct characteristics, DMSs are of interest for a few reasons. Their band parameters can be tuned by changing Mn content, and they have interesting properties combining semimagnetism with semiconductivity, each having well-known uses in electronics, optics, memory functions, etc. It is recognized by now that DMSs serve as a bridge to ferromagnetic semiconductors, and for this reason they are actively studied today.

Among the Mn-based II-VI diluted magnetic semiconductors, $Zn_{1-x}Mn_xTe$ wide-gap alloy is an attractive material for basic investigations and spintronic applications. The ZnTe host is a II-VI semiconductor with a direct band gap E_g of 2.24 eV at $T = 300$ K, corresponding to a green spectral region. The introduction of manganese into ZnTe creates magnetic radiative centers of red luminescence originating in intra-Mn transitions: $^4T_1 \rightarrow {}^6A_1$. Since the gap E_g is wider than the intra-Mn transition energy $E_{Mn} \approx 1.95$ eV, the Mn^{2+} photoluminescence (PL) can be studied in detail in $Zn_{1-x}Mn_xTe$ even in the low-x limit. Bulk $Zn_{1-x}Mn_xTe$ is the only II-VI DMS alloy with $E_g > E_{Mn}$, which has p-type electrical conductivity due to the vacancies of the Zn cation. Because of this property, the excitonic PL from $Zn_{1-x}Mn_xTe$ does not suffer from the PL quenching effect usually observed in n-type DMSs such as $Zn_{1-x}Mn_xSe$. The properties of DMSs are due to the exchange interaction between conduction- and valence-band carriers and paramagnetic ions (s, p-d exchange). In wide-gap DMSs, the result of exchange may be viewed as a very strong enhancement of the external magnetic field to the extent that other effects of the field may be neglected [1–3]. For high hole densities ($p \geqslant 5 \times 10^{24}$ m^{-3}), $Zn_{1-x}Mn_xTe$ becomes a ferromagnetic material [4–6].

In the present work, we investigate $Zn_{1-x}Mn_xTe$, which has been less extensively studied than $Cd_{1-x}Mn_xTe$. Within the optical approach, the most often used experiments were those of magnetoreflectivity and magnetoluminescence. However, there exist no works in which both methods have been used in parallel. It is our purpose to use these methods in order to reveal relations between properties accessible by the two approaches and provide a comprehensive study of the material looking for new effects. In particular, we have in mind properties resulting from the alignment of Mn^{2+} spins in an external magnetic field and those caused by internal optical transitions in single ions. Our study treats the contents of Mn around $x = 0.025$ with low densities of holes, so that interactions between the Mn ions may be neglected. In our optical experiments, we observe pronounced exciton phenomena as well as effects due to residual nonmagnetic impurities. This provides, all in all, quite a rich physical picture of the $Zn_{1-x}Mn_xTe$ DMS.

Our paper is organized as follows. In Sec. II we describe the sample preparation and experimental methods used in the study, Sec. III addresses magnetoreflectivity, and Sec. IV is concerned with magnetophotoluminescence, where we describe separately Mn ions, excitons, and donor-acceptor pairs. The physical contents and works of other authors are

*lkhoi@ifpan.edu.pl

mentioned and discussed in direct connection with the subjects in question, so a separate discussion is not included. The final section contains a summary and conclusion.

II. SAMPLE PREPARATION AND EXPERIMENTAL METHODS

$Zn_{1-x}Mn_xTe$ crystals were grown by the high-pressure Bridgman method from a $(ZnTe)_{1-x}(MnTe)_x$ solution in an evacuated (10^{-6} Torr) quartz ampoule coated with pyrolytic graphite. The ZnTe and MnTe polycrystal sources were synthesized from the 6N purity Zn, Mn, and Te elements. A two-zone vertical Bridgman furnace was used. The hot zone was kept around 1400 °C and the cold zone at 1000 °C to produce a temperature gradient of about 30 °C/cm at the melting point of ZnTe (1295 °C). The ampoule with the $(ZnTe)_{1-x}(MnTe)_x$ powder was initially positioned in the hot zone for 24 h to allow its content to melt completely and then was lowered at the rate of 2.2 mm/h to initiate crystal growth. The growth process was conducted in an atmosphere of nitrogen gas under a pressure of 1 MPa and stopped when the top of the ampoule reached a temperature below 1000 °C. We obtained a large-grain single crystal ingot of 10–14 mm in diameter and about 60 mm long. The $Zn_{1-x}Mn_xTe$ samples split from the as-grown ingot were additionally subjected to annealing at 800 °C and a pressure of 4 MPa of nitrogen gas to improve the composition homogeneity.

The actual Mn content x was determined from the x-ray energy dispersive fluorescence analysis. The x-ray diffraction method was also used to determine the lattice constants of the samples, and it was found that they increased linearly with the actual Mn content in agreement with Vegard's law, $a(x) = 6.101 + 0.206x$ Å. The Hall effect measurements at 300 K showed that the annealed $Zn_{1-x}Mn_xTe$ samples had a hole concentration of $p = 1.08 \times 10^{22}$ m^{-3} and an electrical resistivity of $\rho = 6 \times 10^2$ Ω m; see [7].

For the reflectivity measurements, the incident light was provided by a tungsten-halogen lamp and directed nearly perpendicular to cleaved (110) surfaces of $Zn_{1-x}Mn_xTe$ crystals. The reflected light was detected and analyzed using a quarter-wave plate and a linear polarizer. The magnetophotoluminescence measurements were performed using the 474 nm line of an argon laser. We were able to apply magnetic fields up to 7 T.

III. MAGNETOREFLECTION

As mentioned above, we do not take into account hole-mediated Mn-Mn interaction. According to Ferrand *et al.* [5], for $Zn_{1-x}Mn_xTe$ with Mn content $x = 0.028$ and hole densities $p < 8 \times 10^{23}$ m^{-3} this interaction may be neglected. For our sample having $x = 0.025$ and $p = 1.08 \times 10^{22}$ m^{-3} we are safely below these limits. As a consequence, we consider only the s,p-d exchange interaction between Mn ions and band carriers.

In Fig. 1(a) we show the results of low-temperature photoreflectivity experiments on $Zn_{0.975}Mn_{0.025}Te$ for magnetic fields 0–7 T in the Faraday geometry. The obtained picture is similar to those commonly observed in other wide-gap DMSs. At zero field, the reflectance spectrum exhibits a single line at

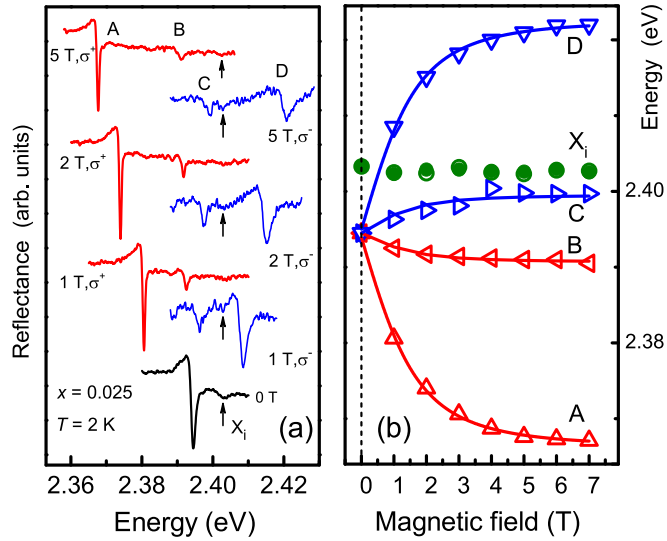

FIG. 1. (a) Reflectance spectra of $Zn_{1-x}Mn_xTe$ with $x = 0.025$ at different magnetic fields in the Faraday geometry for circular light polarizations σ^+ and σ^-. Four resonances are marked with letters on the upper trace. Arrows mark field-independent resonance X_i of unknown origin. (b) Energies of reflectance resonances vs magnetic field. Solid lines are calculated using Eqs. (1) with parameters indicated in the text.

$E_0 = 2.394 \pm 0.00$ eV with a narrow linewidth of ≈ 1.8 meV (plus a weak resonance X_i; see below). This line is attributed to the free exciton X. In a magnetic field, the X line is split into four components: two for σ^+ (A and B) and two for σ^- polarizations (C and D); see the inset in Fig. 2(a). With increasing magnetic field, the exciton resonances are shifted in energy by the exchange interaction with paramagnetic Mn^{2+} ions [2,3].

Figure 1(b) shows displacements of four exciton components A, B, C, and D versus magnetic field, often called the Zeeman shift. They exhibit the typical behavior of wide-gap

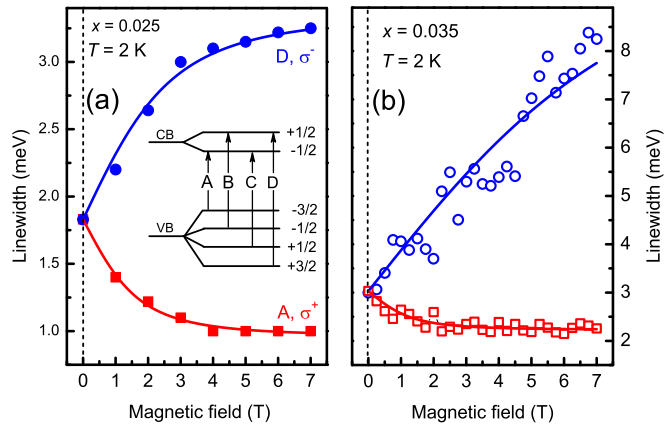

FIG. 2. (a) Resonance linewidths of magnetoreflection resonances for transitions A and D shown in Fig. 1(a) vs magnetic field. Solid lines are fitting curves. The inset indicates schematically magneto-optical transitions between valence and conduction states split by the exchange interaction, as shown in Fig. 1. (b) The same as in (a) but for Mn content $x = 0.035$.

DMSs [2,8]. The energies of the exciton components are given by

$$\begin{aligned} E_A &= E_0 - \tfrac{1}{2}xN_0(\alpha-\beta)\langle S_z\rangle, \\ E_B &= E_0 + \tfrac{1}{2}xN_0\left(\tfrac{1}{3}\beta+\alpha\right)\langle S_z\rangle, \\ E_C &= E_0 - \tfrac{1}{2}xN_0\left(\tfrac{1}{3}\beta+\alpha\right)\langle S_z\rangle, \\ E_D &= E_0 + \tfrac{1}{2}xN_0(\alpha-\beta)\langle S_z\rangle, \end{aligned} \tag{1}$$

where E_0 is the zero-field exciton energy, x is the Mn molar fraction, N_0 is the number of unit cells for unit volume, and $\alpha = \langle S|J|S\rangle$ and $\beta = \langle X|J|X\rangle$ are exchange integrals for conduction and valence bands. The quantity $\langle S_z\rangle$ is the thermal average of the Mn spin component in the z direction, which is described by a modified Brillouin function B_S for the spin value of $S = 5/2$,

$$\langle S_z\rangle = S_0 B_S\left[\frac{g_{\mathrm{Mn}}\mu_B SB}{k_B(T+T_0)}\right], \tag{2}$$

where the Landé factor $g_{\mathrm{Mn}} = 2$, μ_B is the Bohr magneton, k_B is Boltzmann's constant, B is the strength of external magnetic field, T is the temperature, and S_0 and T_0 are adjustable parameters. Using the exchange parameters $N_0\alpha = +0.19$ eV and $N_0\beta = -1.09$ of Ref. [9] and fitting the energies of exciton components to the formulas (1), one can determine the effective spin value S_0 and T_0. We obtain $S_0 = 1.74 \pm 0.02$ and $T_0 = 0.88 \pm 0.02$ K. The value of S_0 is somewhat smaller than the "nominal" value 5/2. The values determined by other authors for $Zn_{1-x}Mn_xTe$ with low Mn contents are $S_0 = 1.88$ for $x = 0.031$ [9] and $S_0 = 1.77$ for $x = 0.032$ [10], while for considerably higher $x = 0.16$ the strongly reduced value of S_0 is 0.5 [11]. We also observed an additional resonance of unknown origin, marked X_i in Figs. 1(a) and 1(b), whose energy does not depend on magnetic field. A similar resonance was observed in $Zn_{1-x}Mn_xSe$ [12].

One can see in Fig. 1(a) that the A resonance for σ^+ polarization not only shifts to lower energies with increasing magnetic field, but it also becomes narrower. On the other hand, the D resonance for the σ^- polarization becomes wider when shifting to higher energies. One can determine the linewidths W in the standard way by measuring the energy distance between the maximum and minimum of the reflectance resonance. In Figs. 2(a) and 2(b), we plot the measured linewidths of the A and D resonances versus B for samples with $x = 0.025$ and 0.035, respectively. It is seen that, for $x = 0.025$, the $W(B)$ dependence resembles the Zeeman shifts shown in Fig. 1(b).

Different field dependences of linewidths in MR resonances were noted in bulk $Cd_{1-x}Mn_xTe$ [8,13] and analyzed theoretically in quantum wells of DMSs. Komarov *et al.* [14] argued that the linewidths of exciton magneto-optical transitions are related to exciton scattering by spin-independent and spin-dependent perturbations. The spin-independent part is related to differences between of electron densities of substitutional atoms and those of the host crystal. The spin-dependent part is caused by the exchange interaction of carriers with unpaired spins of magnetic ions. The Hamiltonian of interaction of an exciton with substitutional ions can be written in the form

$$H_{\mathrm{int}} = \sum_n \frac{1}{N_0}\Big[\left(\Delta_e^{\mathrm{Mn}} - N_0\alpha S_e S_{n,z}\right)\delta(r_e - r_n) + \left(\Delta_h^{\mathrm{Mn}} + \frac{N_0\beta}{3}J_h S_{n,z}\right)\delta(r_h - r_n)\Big]x_n, \tag{3}$$

where N_0 and n are the concentration and coordinates of the cation lattice sites, respectively, $\Delta_{e,(h)}^{\mathrm{Mn}}$ is the potential of nonmagnetic interaction of the electron (hole) with the substitutional Mn ions, $N_0\alpha$ and $N_0\beta$ are defined above, $S_e = \pm 1/2$ and $J_h = \pm 3/2$ are the electron and heavy-hole spin projections on the direction of magnetic field, $S_{n,z}$ is the spin projection of the magnetic ion, and x_n describes the distribution of the impurity ions ($x_n = 0$ if there is a host ion in the nth lattice site and $x_n = 1$ if the site is occupied by a substitutional Mn^{2+} ion).

The difference of exciton scattering for the σ^+ and σ^- circular light components comes from the fact that the initial and final states for the corresponding transitions A and D have different spin orientations appearing in the electron and hole terms: $-N_0\alpha S_e S_{n,z}$ and $+N_0\beta/3J_h S_{n,z}$, respectively. For the A transition there is $S_e = -1/2$ and $J_h = -3/2$, while for the D transition there is $S_e = +1/2$ and $J_h = +3/2$; see the inset in Fig. 2(a). Taking into account that the sign of $N_0\alpha$ is positive and that of $N_0\beta$ negative, and the fact that the sign of $\langle S_z\rangle$ is negative, we obtain that for the A transitions both spin-dependent terms subtract from the spin-independent Δ_e^{Mn}, while for the D transition both terms are sums of spin-dependent and spin-independent terms. As a consequence, for the D transitions the exciton scattering is stronger, which accounts for their larger linewidths. The dependence on the magnetic field comes from the fact that, in the mean-field approach, the substitutional ion content x_n and the manganese spin orientations $S_{n,z}$ in Eq. (2) can be replaced by their average values x and $\langle S_z\rangle$, respectively. As a consequence, the linewidths are directly related to $\langle S_z\rangle$ and thus depend on magnetic field.

Finally, it is seen in Fig. 2(b) that for a $Zn_{1-x}Mn_xTe$ sample with higher Mn content ($x = 0.035$), the linewidths of reflectivity resonances are distinctly larger than those shown in Fig. 2(a). This is understandable as seen by Eq. (3) because it corresponds to a higher number of spin-scattering Mn ions.

IV. MAGNETOPHOTOLUMINESCENCE

We have performed magnetophotoluminescence (MPL) experiments on $Zn_{1-x}Mn_xTe$. They were carried in Faraday geometry, and the luminescent light was analyzed for the left and right circularly polarized components. Figure 3 shows the overall MPL spectrum without magnetic field as well as at $B = 1$ and 6 T versus photon energy below the energy gap of $Zn_{1-x}Mn_xTe$ for low Mn content $x = 0.025$. Beginning with high energies, the main structures of the MPL spectrum are due to excitons between 2.4 and 2.35 eV, donor-acceptor pairs between 2.35 and 2.1 eV, and Mn^{2+} ions between 2.1 and 1.7 eV. The striking feature of the spectrum is that *all three structures gain in intensity with increasing magnetic field*. This overall picture, exhibiting three different physical entities, not

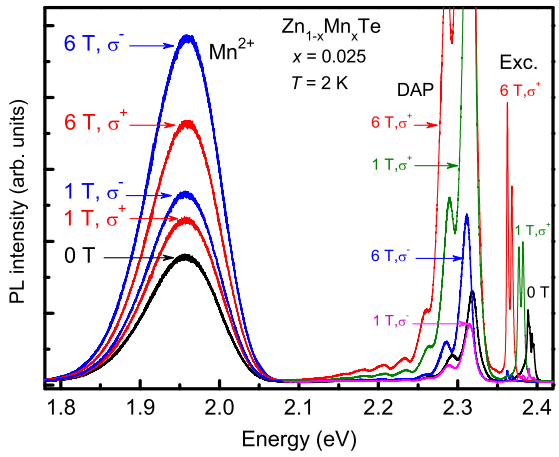

FIG. 3. Magnetophotoluminescence (MPL) spectrum of $Zn_{1-x}Mn_xTe$ at different magnetic fields in the Faraday geometry for circular light polarizations σ^+ and σ^-. Going from high to low energies, MPL due to excitons, donor-acceptor pairs, and internal recombination of Mn^{2+} ions is observed. All structures are strongly enhanced by magnetic field.

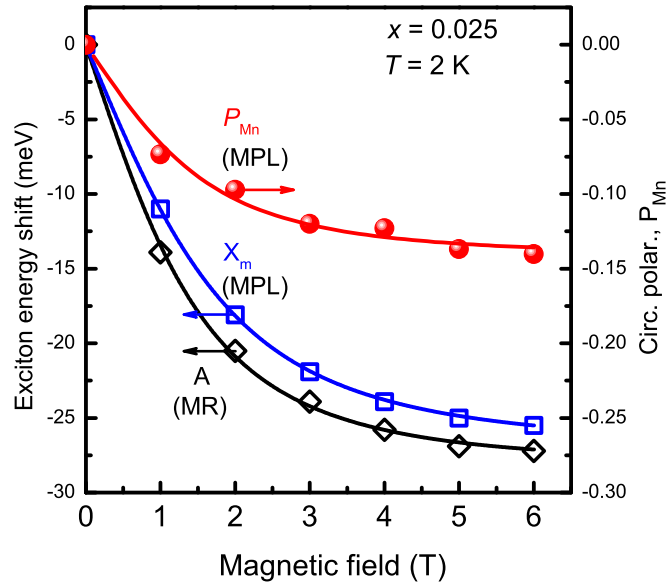

FIG. 4. Degree of circular polarization P_{Mn} for Mn^{2+} emission as defined in Eq. (4) (right scale), exciton energy shifts of X_m peak from MPL (left scale), and A resonance from MR (left scale) vs magnetic field. Solid lines are drawn to guide the eye.

observed simultaneously on other DMS, is one of the main results of our study.

A. Spin-polarized MPL due to Mn ions

We first consider MPL due to internal $3d$-*shell* electron recombination of Mn^{2+} ions. It originates from optical transitions between the excited ion state $^4T_1$ and the ground state $^6A_1$. Such transitions are in principle not allowed in the dipole approximation, but this rule is relaxed by the spin-orbit interaction and the lack of inversion symmetry of the crystal environment [3,15–17]. The mechanism of energy transfer from excitons to the Mn^{2+} ions is still not quite clear [18–21], and we do not go into the details of this problem.

In the presence of a magnetic field, left and right circular light polarizations in the Faraday configuration excite different transitions between the ground and excited states of Mn^{2+} ions. Fournier *et al.* [15] considered absorption transitions between the ground sextuplet $^6A_1$ ($S = 5/2$) and the quadruplet of $^4T_1$ ($S = 3/2$), and they deduced the selection rules $\Delta m_s = \pm 1$ for the two light polarizations, where m_s are quantized projections of the angular momentum in the field direction z. Van Gorkom [16] and Baryshnikov *et al.* [17] took into account the tetrahedral field environment of the Mn ions by attributing to the excited states the orbital angular momentum $L = 1$. Then, taking into account the spin-orbit interaction, one obtains in the "pseudo J" formalism the excited states with the total angular momentum $J' = 5/2, 3/2, 1/2$. The selection rules for transitions of σ^+ and σ^- polarizations are $m'_s = m_s \pm 1$, respectively. In Ref. [17], the transitions from the $J' = 1/2$ doublet were omitted.

The total MPL intensity related to Mn^{2+} is $I_{\mathrm{tot}} = I^+ + I^-$, where I^+ and I^- denote intensities for the left (σ^+) and right (σ^-) circular polarizations (red and blue lines in Fig. 3, respectively). It is then clear that the overall increase of the intensity at $B = 6$ T, as compared to that at $B = 0$, is considerable. This is in contrast to the behavior of other DMSs (see below). We first consider the circularly polarized magnetophotoluminescence from Mn^{2+} and the Zeeman energy shift of the MR exciton components ΔE_i ($i = A, B, C, D$). The degree of circular polarization of the Mn^{2+} emission, denoted as P_{Mn}, is defined as

$$P_{\mathrm{Mn}} = \frac{I^+ - I^-}{I^+ + I^-}. \tag{4}$$

Figure 4 shows P_{Mn} versus magnetic field for $0 \leqslant B \leqslant 6$ T (right scale) and the exciton energy shift ΔE_{X_m} (as observed in MPL), as well as that observed in magnetoreflectivity for the A component ΔE_A shown in Fig. 1(b) (left scale). The exciton energy shifts observed in MPL and reflectivity practically coincide, which is understandable since they are manifestations of the same phenomenon observed by different techniques. On the other hand, the exciton energy shifts (all components) are proportional to P_{Mn}. To demonstrate this property, we show in Fig. 5 the Zeeman shifts of exciton energies plotted versus P_{Mn} values. The linear relation between all four Zeeman shifts ΔE_i ($i = A, B, C, D$) and P_{Mn} indicates that not only the Zeeman shifts but also the degree of circular polarization P_{Mn} track the magnetization of the Mn subsystem: $M = -N_0 x g_{\mathrm{Mn}} \mu_B \langle S_z \rangle$. We can write the following for a specific Zeeman energy shift (say, A transition): $\Delta E_A = \gamma P_{\mathrm{Mn}}$, from which one can determine the factor γ using the slope of the corresponding straight line in Fig. 5. For $x = 0.025$, the values of γ are $\mp 0.199 \pm 0.001$ and $\mp 0.03 \pm 0.01$ for A, D and B, C MR exciton components, respectively. We can now go back to Eq. (1) and write for the A component

$$P_{\mathrm{Mn}} = \frac{N_0(\alpha - \beta)x}{\gamma} \langle S_z \rangle. \tag{5}$$

The above equality relates the thermal average of the Mn spin component $\langle S_z \rangle$, which is the mean-field collective property of all Mn^{2+} ions in the sample, to the degree of circular polarization P_{Mn} related to the individual property of

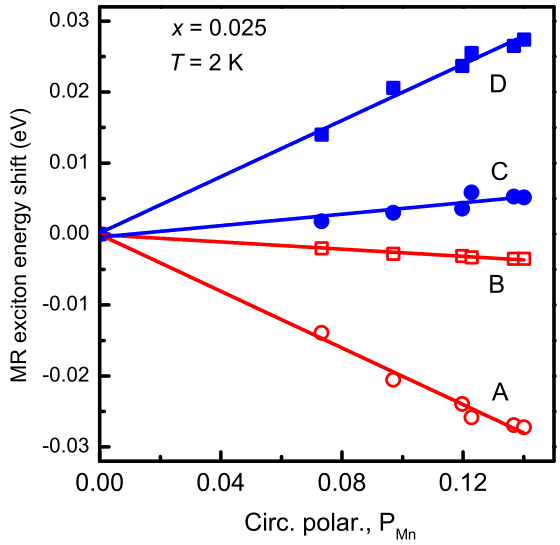

FIG. 5. Exciton Zeeman energy shifts of four reflectivity components shown in Fig. 1(b) (vertical scale) plotted against P_{Mn} values for the corresponding fields (horizontal scale). The resulting straight lines demonstrate that all four Zeeman shifts are proportional to P_{Mn}.

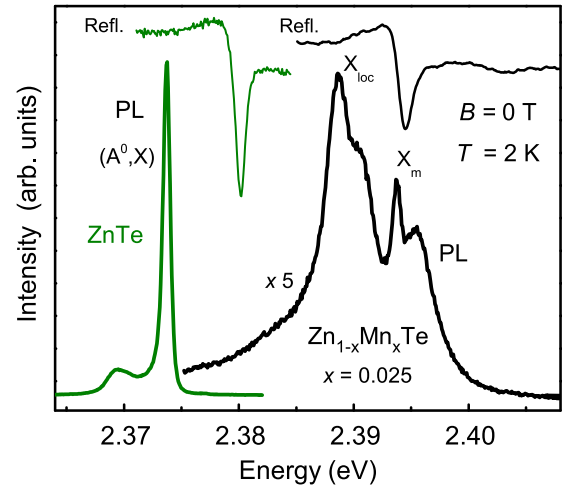

FIG. 6. Exciton photoluminescence and reflectance spectra measured at 2 K for ZnTe and $Zn_{0.975}Mn_{0.025}Te$, the PL peak X_m is due to mobile excitons (this is confirmed by the corresponding reflectance structure), while X_{loc} is due to excitons localized by alloy potential fluctuations. For ZnTe, the free-exciton photoluminescence is not observed, while the PL peak (A^0, X) at lower energy is due to excitons localized by neutral acceptors.

single Mn^{2+} ions. We conclude that the low-temperature P_{Mn} is an important quantity characterizing a dilute magnetic semiconductor. We consider this finding an important result of our study. Khoi *et al.* [22] measured the temperature dependence of the Mn-related photoluminescence in $Zn_{1-x}Mn_xTe$ at $B = 0$ showing that it is almost completely quenched at $T = 80$ K. Fournier *et al.* [15] in an early work describing ZnS doped with Mn^{2+} showed that the P_{Mn} can be described by the Jahn-Teller model for the Mn^{2+} ions.

In this connection, one should mention the work of Visvantha *et al.* [23], who studied MPL in bulk ZnSe:Mn and colloidal nanocrystals ZnSe/CdSe:Mn. In contrast to our data, in the ZnSe:Mn case both σ^+ and σ^- components of MPL due to Mn^{2+} strongly decreased with B and showed no polarization. However, for colloidal nanocrystals, the Mn^{2+} emission was circularly polarized and P_{Mn} was proportional to the magnetization of the sample. This result is similar to ours. Muller and Gebhardt [24] observed PL in $Zn_{1-x}Mn_xTe$ related to electron recombination of Mn ions without magnetic field, while Baryshnikov *et al.* [17] observed the spin-polarized MPL related to Mn^{2+} ions in bulk $Cd_{1-x}Mn_xTe$ with $x \geqslant 0.36$.

B. Spin-polarized MPL due to excitons

Now we turn to the exciton photoluminescence shown at the highest energies in Fig. 3. We begin with the results for $B = 0$ shown in Fig. 6 together with the reflectivity structures. For ZnTe (green lines) one observes in the reflectivity a free-exciton resonance at 2.3795 eV, while the PL peak at 2.3736 eV is related to the exciton trapped at a neutral Zn-vacancy acceptor [25] having a binding energy of 5.9 meV. For $Zn_{1-x}Mn_xTe$ (black lines), both reflectivity and PL spectra are shifted to higher energies (since the gap is larger) and the PL structure is considerably richer. It consists of two strong lines X_{loc} and X_m. Each of these lines has a weak shoulder on the high-energy side that disappears upon the application of a magnetic field. Their assignment is not quite clear but, judging by the corresponding reflectivity resonance and taking into account the case of $Zn_{0.955}Hg_{0.045}Te$ reported in Ref. [26], the high-energy peak is the signature of the mobile excitons X_m, while the low-energy one X_{loc} is attributed to the exciton localized by the potential fluctuations due to substitution of Mn^{2+} for Zn^{2+} ions.

Figure 7(a) shows the PL spectra for increasing magnetic fields in semilogarithmic graphs for σ^+ and σ^- polarizations. It is seen that the σ^+ spectra show two pairs of lines: X^A_{loc} and X^A_m in the energy range of the reflectivity component A, and X^B_{loc} and X^B_m in the energy range of the component B. The energies of X^A_m and the A component of MR coincide almost exactly, which is understandable since they correspond to the same transition measured by MPL and MR methods, respectively. The intensities of X^A_{loc} and X^A_m increase monotonically with the field (see also Fig. 3). These features show the validity of exciton identification. The potential fluctuations in $Zn_{1-x}Mn_xTe$ make the exciton PL spectrum strongly different from that of ZnTe. A similar excitonic structure in MPL experiments was observed on $Zn_{1-x}Mn_xSe$ [27]. The σ^- spectrum recorded at 1 T shows a weak line corresponding to the C reflectance exciton component and four weak lines at the same energy positions as those for the σ^+ polarization. This is because the σ^- polarization contains a small admixture of σ^+; cf. [28]. In other words, for each magnetic-field value both σ^+ and σ^- MPL structures (marked with red and blue) are in fact the same structures of different intensities corresponding to the σ^+ polarization. Exciton peaks for σ^- polarization would occur at higher energies. We observe, all in all, four peaks at low fields and three peaks at higher fields. We also observe the MPL peak corresponding to the MR component B [marked with red diamond in Fig. 7(b)], but only for the field $B = 1$ T.

The energies of the three MPL peaks and of all four reflectance resonances are plotted in Fig. 7(b) for magnetic

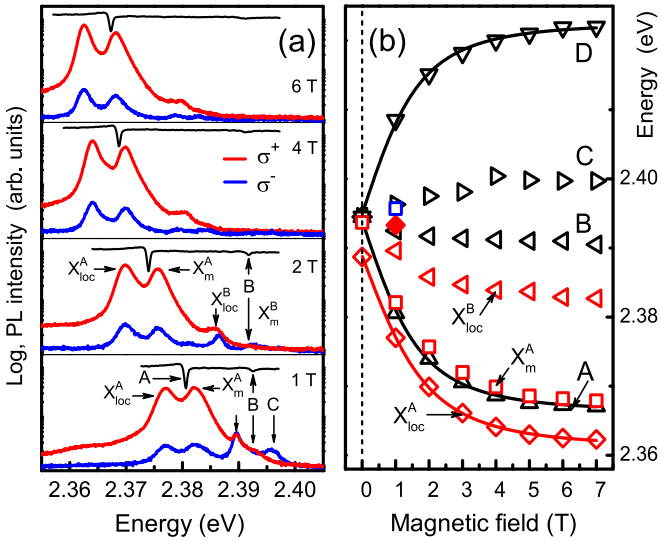

FIG. 7. (a) Excitonic MPL spectra of $Zn_{0.975}Mn_{0.025}Te$ recorded at $B = 1$, 2, 4, and 6 T in σ^+ and σ^- polarizations and plotted in semilogarithmic graphs. Peaks for σ^- polarization have very low intensity and are due to mixing of σ^+ and σ^- polarizations. The corresponding A component of magnetoreflectivity is also shown. (b) Energies of excitonic MPL peaks and MR components A, B, C, and D vs magnetic field. The energy of the X_m MPL peaks coincides almost exactly with that of the A component of MR. The field-independent resonance [marked in green in Fig. 1(b)] is omitted here.

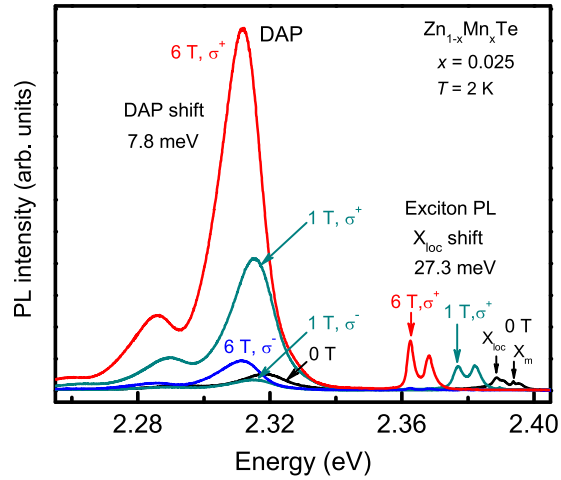

FIG. 8. Magnetophotoluminescence in $Zn_{1-x}Mn_xTe$ related to the donor-acceptor pairs (DAPs) and excitons vs energy at different magnetic fields. The DAP peaks for σ^- polarization have very low intensity and are excited only because σ^- polarization has a small admixture of σ^+. The downward energy shift of DAP peaks with increasing magnetic field is much smaller than that of the exciton peaks; see the text.

fields of $0 \leqslant B \leqslant 7$ T. We associate the transitions marked $X^B_{\rm loc}$ and $X^A_{\rm loc}$ with corresponding excitons B and A localized by potential fluctuations. We observe the field increase of energy differences between the free exciton B and the localized one $X^B_{\rm loc}$, and similarly for A and $X^A_{\rm loc}$. As the magnetic field increases, the exciton orbit shrinks and the electrostatic interaction with the potential fluctuation becomes enhanced. As a consequence, the binding energy increases. This behavior is analogous to the increase of donor binding energy with magnetic field commonly observed in nonmagnetic semiconductors; see Refs. [29] and [30].

The increase of exciton binding energy with the field, seen in Fig. 7(b), is bigger for transitions B than those of A. This feature can have experimental reasons since the peaks $X^A_{\rm loc}$ and X^A_m in Fig. 7(a) are distinct and have equal intensity, while the peak $X^B_{\rm loc}$ is much smaller, appears on the shoulder, and, consequently, its position is not determined too well. On the other hand, the difference of binding energies for excitons A and B, if real, can be due to the difference of exciton effective masses: heavy-hole for the exciton A and light-hole for B. It could also be caused by an interaction of the type described in Eq. (3). This observation requires further studies. MPL excitonic structures, similar to those shown in Fig. 7(a), were observed by Hayes *et al.* [11] for $Zn_{1-x}Mn_xTe$ and by Nakahara *et al.* [31] for $Cd_{1-x}Mn_xTe$.

To conclude the above subsection, we emphasize three effects. First, the introduction of Mn atoms makes the MPL excitonic spectrum more involved. Here again, parallel results on reflectivity facilitate identification of additional structures; see Fig. 6. Second, mixing of σ^+ and σ^- circular light polarizations, resulting most probably from experimental imperfections, is clearly demonstrated; see Fig. 7(a). Third, the increase of binding energies with magnetic field for excitons localized by potential fluctuations is shown; see Fig. 7(b).

C. MPL due to donor-acceptor pairs

Although nonmagnetic impurities in $Zn_{1-x}Mn_xTe$ are not our main interest, we mention a few features of the MPL spectrum related to them. It is known that acceptors in ZnTe originate mostly from Zn vacancies, so that we deal with donor-acceptor pairs (DAPs). It is seen in Fig. 3 that the increase of luminescence due to magnetic field is particularly large for peaks related to DAPs observed between 2.1 and 2.35 eV. This feature was observed in ZnSe [32]. We observe a relative energy stability of the DAP peak of MPL with respect to magnetic field intensity, as illustrated in Fig. 8. As the field increases from 0 to 6 T, the DAP peak shifts to lower energies by 7.8 meV, i.e., much more slowly than the exciton peak for which the corresponding shift is 27.3 meV. A similar behavior was observed in other DMS materials [33]. Godenko *et al.* [34] interpreted this relative stability of DAP energy in $Zn_{1-x}Mn_xSe$ as a suppression of the Zeeman shift for DAPs and described it with a model in which the impurity wave functions were written as sums of extended and localized components. The extended component characterizes shallow donors while the localized one acceptors. An extended portion of the function "sees" many Mn ions and is susceptible to the Zeeman shift, whereas the localized one "sees" very few (or none) Mn ions, so the shift is strongly suppressed. This description explained the overall suppression of the Zeeman shift for the donor-acceptor pairs. The above model can be used to explain our $Zn_{1-x}Mn_xTe$ results.

As to the possible influence of bound magnetic polarons, it is known [35,36] that moderately strong magnetic fields suppress magnetic polaron formation, so the polaron effect does not intervene in our case. A similar conclusion was

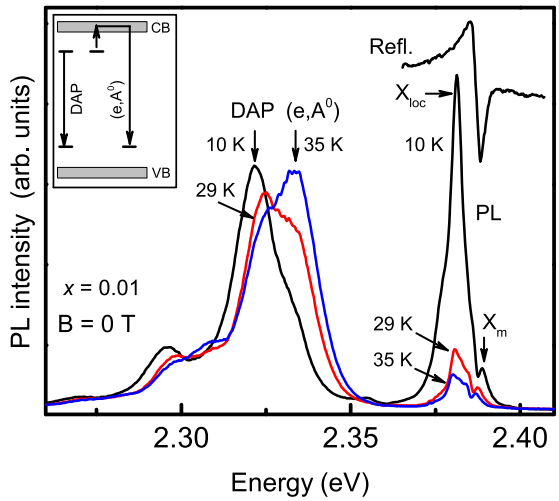

FIG. 9. Photoluminescence due to DAP transitions, as well as free and bound excitons in $Zn_{0.99}Mn_{0.01}Te$ at $B = 0$ for various temperatures T. With increasing T, the DAP peak shifts upward in energy and a free-to-bound peak emerges (see the inset). In parallel, the relative intensities of free-to-localized exciton peaks increase. The low-temperature reflectance spectrum related to free and localized excitons is shown for comparison.

reached by Godenko *et al.* [34] for DAP photoluminescence in $Zn_{1-x}Mn_xSe$.

Finally, in Fig. 9 we show luminescence related to donor-acceptor pairs and excitons in the $Zn_{1-x}Mn_xTe$ sample with $x = 0.01$ at zero magnetic field and different temperatures. As the temperature increases, the free-to-bound PL peak emerges at higher energies because electrons are excited from shallow donors to the conduction band and the recombination occurs from the latter; see the inset. This measurement allows us to determine the acceptor energy. The energy gap is $E_g = E_X + E_b$, where E_X is the exciton energy determined from the reflectivity and E_b is the exciton binding energy. The reflectivity data in Fig. 9 give $E_X = 2.387$ eV while the exciton binding energy is $E_b = 13.2$ meV [37], so that $E_g = 2.400$ eV. The PL peak at 35 K occurs at $\hbar\omega = 2.334$ eV. The luminescence energy in a free-to-bound optical transition is given by [38]

$$\hbar\omega = E_g - E_A + \frac{1}{2}k_BT, \tag{6}$$

where E_A is the acceptor binding energy. From Eq. (6) we get $E_A = 67.5$ meV for $Zn_{1-x}Mn_xTe$ with $x = 0.01$. The above reasoning shows once again the advantage of parallel reflectivity and luminescence investigations. We add that it is difficult to measure the acceptor binding energy in undoped ZnMnTe using the transport method because at low temperatures the material has very high resistance.

As to the PL peaks at higher energies related to excitons, shown in Fig. 9, at 10 K we observe a mobile exciton X_m (this is confirmed by the energy coincidence with the reflectivity) and a strong peak due to excitons bound to the potential fluctuations X_{loc}. As the temperature increases, both exciton peaks decrease, which is due to the standard thermal scattering. However, one observes in addition that the ratio of strengths of X_{loc} to X_m excitons quickly decreases since the former are delocalized by thermal excitations.

V. SUMMARY AND CONCLUSION

Magnetoreflectivity and magnetophotoluminescence in $Zn_{1-x}Mn_xTe$ are measured and analyzed in parallel. Complementary investigations of MR and MPL make it possible to relate properties characterizing mean-field behavior to the individual behavior of Mn^{2+} ions. It is remarked that linewidths of resonances observed in MR differ for various magneto-optical spin transitions and depend on magnetic-field intensity. This effect is analyzed in terms of spin-dependent exciton scattering. It is observed that all three parts of the MPL spectrum, related to Mn^{2+} ions, donor-acceptor pairs, and excitons, are strongly enhanced by an external magnetic field. It is shown that the Zeeman shifts of all four MR resonances are proportional to the low-temperature degree of circular polarization P_{Mn} related to Mn^{2+} ions. The latter is thereby established as an important quantity characterizing a diluted magnetic semiconductor. The effects of mixing the left and right circular light polarizations are observed in the exciton structures of MPL. An increase of binding energies with growing magnetic field for excitons localized by potential fluctuations is demonstrated and interpreted. A relative energy stability of donor-to-acceptor MPL excitations as functions of magnetic field is observed and analyzed. The temperature evolution of the MPL spectrum related to DAP excitations is observed and used to determine the acceptor binding energy in $Zn_{0.99}Mn_{0.01}Te$. All in all, the presented optical analysis of $Zn_{1-x}Mn_xTe$ can serve as a model for the comprehensive characteristics of a diluted magnetic semiconductor.

We conclude that in many ways $Zn_{1-x}Mn_xTe$ is a typical diluted magnetic semiconductor. However, the comprehensive study with the parallel use of magnetoreflectivity and magnetophotoluminescence not only confirmed various properties observed in other DMS materials, but it also revealed unexpected features and new effects. Some of these new phenomena are not yet well understood and require further investigation.

ACKNOWLEDGMENTS

One of the authors (L.V.K.) wishes to thank Professor J. Kossut of the Polish Academy of Sciences, Professor J.K. Furdyna of the University of Notre Dame, and Professor J. Geurts of the University of Wurzburg for making available their experimental facilities for magneto-optical measurements.

[1] A. V. Komarov, S. M. Ryabchenko, O. V. Terletskii, I. I. Zheru, and R. D. Ivanchuk, Zh. Eksp. Teor. Fiz. **73**, 608 (1977) [Sov. Phys. JETP **46**, 318 (1977)].

[2] J. Gaj, J. Ginter, and R. R. Gałązka, Phys. Status Solidi B **89**, 655 (1978).

[3] J. K. Furdyna, J. Appl. Phys. **64**, R29 (1988).

[4] L. Van Khoi, M. Sawicki, K. Dybko, V. Domuchovski, T. Story, T. Dietl, A. Jedrzejczak, J. Kossut, and R. R. Gałązka, Phys. Status Solidi B **229**, 53 (2002).
[5] D. Ferrand, J. Cibert, A. Wasiela, C. Bourgognon, S. Tatarenko, G. Fishman, T. Andrearczyk, J. Jaroszyński, S. Koleśnik, T. Dietl, B. Barbara, and D. Dufeu, Phys. Rev. B **63**, 085201 (2001).
[6] H. Kępa, V. K. Le, C. M. Brown, M. Sawicki, J. K. Furdyna, T. M. Giebultowicz, and T. Dietl, Phys. Rev. Lett. **91**, 087205 (2003).
[7] To determine hole concentration in a highly doped sample, one should measure the Hall effect at low temperatures and high magnetic fields where the sample magnetization saturates. However, it was found for $Zn_{1-x}Mn_xTe$ (see Ref. [5]) that a contribution from the anomalous Hall effect is very small at room temperature and the Hall resistivity is linear in a magnetic field B at temperatures above 150 K. Also, the slopes of B dependences of the Hall resistivities at room temperature and at low temperatures are identical at high B values. These experimental facts allow us to use the Hall resistivity at room temperature to determine hole concentration in $Zn_{1-x}Mn_xTe$.
[8] A. V. Komarov, S. M. Ryabchenko, and N. I. Vitrikhovskii, Pis'ma Zh. Eksp. Teor. Fiz. **27**, 441 (1978) [Sov. Phys. JETP Lett. **27**, 413 (1978)].
[9] A. Twardowski, P. Świderski, M. von Ortenberg, and R. Pauthenet, Solid State Commun. **50**, 509 (1984).
[10] G. Barilero, C. Rigaux, M. Menant, N. H. Hau, and W. Giriat, Phys. Rev B **32**, 5144 (1985).
[11] W. Hayes, M. J. McNamee, and D. J. Mowbray, J. Phys. C **21**, L1065 (1988).
[12] W. Y. Yu, A. Twardowski, L. P. Fu, A. Petrou, and B. T. Jonker, Phys. Rev. B **51**, 9722 (1995).
[13] S. M. Ryabchenko, Yu. G. Semenov, and O. V. Terletskii, Fiz. Tverd. Tela **27**, 2901 (1985) [Sov. Phys. Solid State **27**, 1746 (1985)].
[14] A. V. Komarov, V. I. Sugakov, G. V. Vertsimakha, W. Zaleszczyk, G. Karczewski, and T. Wojtowicz, J. Phys: Condens. Matter **18**, 7401 (2006).
[15] D. Fournier, A. C. Boccara, and J. C. Rivoal, J. Phys. C **10**, 113 (1977).
[16] G. G. P. van Gorkom, Solid State Commun. **11**, 1253 (1972).
[17] K. A. Baryshnikov, L. Langer, I. A. Akimov, V. L. Korenev, Yu. G. Kusrayev, N. A. Averkiev, D. R. Yakovlev, and M. Bayer, Phys. Rev. B **92**, 205202 (2015).
[18] V. G. Abramishvili, A. V. Komarov, S. M. Ryabchenko, and Yu. G. Semenov, Solid State Commun. **78**, 1069 (1991).
[19] M. Nawrocki, Yu. G. Rubo, J. P. Lascaray, and D. Coquillat, Phys. Rev. B **52**, R2241 (1995).
[20] H. Falk, J. Hubner, P. J. Klar, and W. Heimbrodt, Phys. Rev. B **68**, 165203 (2003).
[21] A. V. Chernenko,, P. S. Dorozhkin, V. D. Kulakovskii, A. S. Brichkin, S. V. Ivanov, and A. A. Toropov, Phys. Rev. B **72**, 045302 (2005).
[22] L. V. Khoi, J. Kossut, and R. R. Gałązka, J. Supercond. **16**, 427 (2003).
[23] R. Viswanatha, J. M. Pietryga, V. I. Klimov, and S. A. Crooker, Phys. Rev. Lett. **107**, 067402 (2011).
[24] E. Muller and W. Gebhardt, Phys. Status Solidi B **137**, 259 (1986).
[25] T. Taguchi, S. Fujita, and Y. Inuishi, J. Cryst. Growth **45**, 204 (1978).
[26] H. Mariette, R. Triboulet, and Y. Marfaing, J. Cryst. Growth **86**, 558 (1988).
[27] A. V. Komarov, S. M. Ryabchenko, and Yu. G. Semenov, Pis'ma Zh. Eksp. Teor. Fiz. **54**, 82 (1991) [Sov. Phys. JETP Lett. **54**, 79 (1991)].
[28] N. T. Khoi, J. Ginter, and A. Twardowski, Phys. Status Solidi B **117**, 67 (1983).
[29] Y. R. Yafet, R. W. Keyes, and E. N. Adams, J. Phys. Chem. Solids **1**, 137 (1956).
[30] W. Zawadzki, in *Landau Level Spectroscopy*, edited by G. Landwehr and E. I. Rashba (North Holland, Amsterdam, 1991), p. 1305.
[31] J. Nakahara, T. Nouchi, H. Arai, I. Mogi, G. Kido, and J. Watanabe, J. Cryst. Growth **117**, 830 (1992).
[32] B. C. Cavenett and W. E. Hagston, Solid State Commun. **16**, 1235 (1975).
[33] A. V. Komarov, S. M. Ryabchenko, O. V. Terletskii, R. D. Ivanchuk, and A. V. Savitskii, Fiz. Tekh. Poluprovodn. **14**, 17 (1980) [Sov. Phys. Semicond. **14**, 9 (1980)].
[34] L. P. Godenko, M. A. Ivanov, and A. V. Komarov, Zh. Eksp. Teor. Fiz. **105**, 708 (1994) [Sov. Phys. JETP **78**, 378 (1994)].
[35] V. F. Aguekian, L. K. Gridneva, and A. Yu. Serov, Solid State Commun. **85**, 859 (1993).
[36] Y. G. Kusrayev, K. V. Kavokin, G. V. Astakhov, W. Ossau, and L. W. Molenkamp, Phys. Rev. B **77**, 085205 (2008).
[37] H. Venghaus and P. J. Dean, Phys. Rev. B **21**, 1596 (1980).
[38] L. Pavesi and M. Guzzi, J. Appl. Phys. **75**, 4779 (1994).